Refractive index sensing with an air-slot photonic crystal nanocavity

Jana Jágerská,* Hua Zhang, Zhaolu Diao, Nicolas Le Thomas, and Romuald Houdré

*Institut de Physique de la Matière Condensée, Ecole Polytechnique Fédérale de Lausanne (EPFL),
Station 3, CH-1015 Lausanne, Switzerland*
Corresponding author: jana.jagerska@epfl.ch

We investigate an air-slot photonic crystal cavity for high-precision refractive index sensing. The high quality factor $\sim 2.6 \times 10^4$ of the cavity, along with a strong overlap between the resonant mode and the hollow core region, allows us to achieve an experimental sensitivity of 510 nm per refractive index unit (RUI) and a detection limit below 1×10^{-5} RUI. The device has a remarkably low sensing volume of 40 aliters, holding less than 1×10^6 molecules.   © 2010 Optical Society of America
OCIS codes: 230.3120, 230.5298, 280.4788.

Optical cavities realized in a photonic crystal (PhC) environment allow for both high quality factors $Q \sim 10^6$ and strong field confinement [1,2], resulting in enhanced light–matter interaction within an extremely small volume. They find a vast number of applications in nonlinear physics, quantum electrodynamics and, based on experimental demonstrations achieved to date, they also constitute a promising building block for optical sensors [3,4]. However, in typical PhC cavities, strong light–matter interaction occurs in the high-index material where the majority of the optical field is located, making it difficult to efficiently probe the physical properties of analyte found within the hollow part of the cavity. This drawback can be overcome with the use of an air-slot cavity, i.e., a PhC cavity with a nanometer-wide slot designed in the cavity defect region [see Fig. 1(a)]. Because of a large electric field discontinuity at the slot boundaries [5], such a cavity can confine TE-polarized modes in the slot, thus allowing for a large interaction of the optical field with the low-index medium.

The air-slot cavity was first proposed in a one-dimensional photonic crystal by Robinson *et al.* [6], followed by several different designs in PhC slabs [7,8]. However, the full potential of the structure for sensitive on-chip detection has not yet been clearly assessed. In this Letter, we experimentally investigate a new type of a PhC air-slot cavity and demonstrate that it can act as a high-precision gas index sensor.

Figure 1(a) shows a typical air-slot PhC cavity, which is based on a W1 waveguide with an air-slot embedded in the line-defect region. To create a cavity, one can either modify the properties of the PhC mirror or the dimensions of the slot itself. The first approach was adopted by Di Falco *et al.* [7], who locally reduced the lattice constant of the photonic crystal to create a heterostructure cavity, as well as by Yamamoto *et al.* [8] and Gao *et al.* [9], where the holes adjacent to the slot were transversely shifted to form a width-modulated line-defect cavity. In the present design, the PhC lattice is kept unchanged, but the width of the air slot is locally reduced by 20 nm to delimit the volume of the cavity [insert of Fig. 1(a)]. Reduced-slit width results in the formation of reflective barriers for the cavity mode, as can be inferred from the dispersion diagram of the slot PhC waveguides shown in

Fig. 1(b). When opening an air-slot inside the W1 defect region, the TE-polarized slot waveguide mode is lifted up from the dielectric band, shifting the mode cutoff to higher frequencies as the width of the slit increases. Consequently, the 120 nm slot waveguide mode lies at slightly higher frequencies than the 100 nm one, supporting a defect state when sandwiched between two 100 nm slot waveguide sections. The theoretical dispersion was calculated by the guided-mode expansion method [10] for a photonic crystal with a lattice constant $a = 510$ nm and a filling factor $f = 0.4$.

We focus on a cavity with a length equal to three lattice constants $L = 3a$, the resonant state of which is found between the cutoffs of the 120 and 100 nm wide slot waveguides. The corresponding electric field distribution plotted in the inset of Fig. 1(b) confirms that the cavity
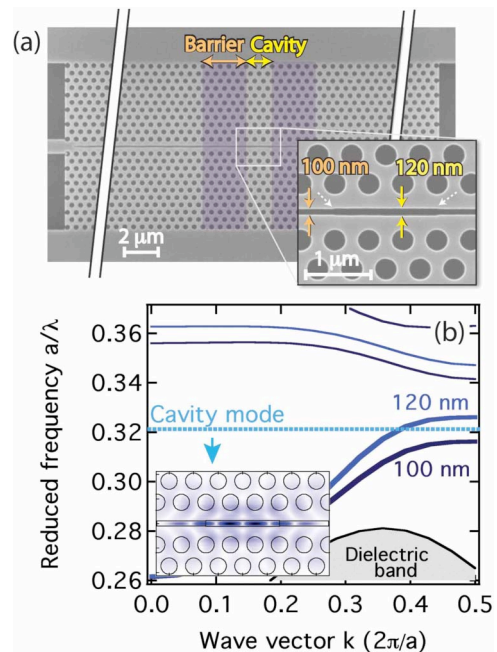

Fig. 1. (Color online) (a) Scanning electron microscopy image of the air-slot cavity. (b) Theoretical dispersion curves of the 100 and 120 nm PhC slot waveguides (solid line) shown together with the air-slot cavity resonance (dashed line). Inset: electric field distribution $|E_{xy}|$ of the cavity mode.

© 2010 Optical Society of America

mode is strongly confined within the slot region, having an effective mode volume [2] equal to $V_{\text{eff}} = 0.05 \ \mu\text{m}^3$ and the spatial overlap Γ with the gas as high as 0.83. Knowing the mode field overlap Γ, the first-order perturbation theory can be used to estimate the sensitivity S of the device to the refractive index change Δn inside the slot [11]:

$$S = \frac{\Delta\lambda}{\Delta n} = \Gamma \frac{\lambda}{n_{\text{eff}}}, \tag{1}$$

where λ is the resonance wavelength of the cavity and $n_{\text{eff}}^2 = \Gamma n_{\text{gas}}^2 + (1 - \Gamma) n_{\text{Si}}^2$ is the effective index experienced by the cavity mode. For resonance frequency $\lambda = 1570$ nm, $n_{\text{gas}} = 1$, and $n_{\text{Si}} = 3.47$, we get a sensitivity of $S = 770$ nm per refractive index unit (RIU), which is quite remarkable for a sensor with an active sensing volume as low as $0.04 \ \mu\text{m}^3 = 40$ aliters.

The proposed air-slot cavity was processed on a 220 nm thick silicon-on-insulator wafer (SOI from Soitec, France) with a 2 μm buried oxide layer. The ZEP-520A positive-tone electron-beam resist was used as the etching hard mask, and the transfer of the pattern from the ZEP to the Si core layer was performed in a single step, using inductively coupled plasma (ICP) etching with a gas combination of SF_6 and C_4F_8. The 2 μm thick buried oxide layer was removed by etching for 30 min in fluoric-based acid to achieve a freestanding silicon membrane. Supercritical drying was performed to avoid strain in the membrane structure.

The fabricated device was characterized using a setup shown in Fig. 2(a), which combines the end-fire technique with optical imaging [12]. The air-slot cavity is excited using a TE-polarized, monochromatic diode laser tunable in the wavelength range of 1470–1660 nm. The optical signal is coupled through a lensed fiber and adiabatically tapered access waveguides into the PhC structure and finally through a $5a$ long barrier region into the cavity [see Fig. 1(a)]. The length of the barriers was carefully chosen to achieve a high loaded Q factor while keeping the transmission at a detectable level. In parallel with the standard end-fire transmission measurement, the light emitted from the sample surface is collected by a high numerical aperture (NA = 0.8) microscope objective and detected with an infrared CCD camera. Direct imaging of the sample surface yields the real-space image, which allows us to monitor the optical field distribution at the cavity. Furthermore, by imaging the back-focal plane of the collecting lens, we can access the far-field image, which gives the angular emission spectrum of light radiated from the cavity.

The experimental transmission spectrum of the air-slot cavity is shown in Fig. 2(b). The cavity barriers are transparent down to 1590 nm, where the mode cutoff of the 100 nm wide slot waveguide is found. Approximately 20 nm below this cutoff, we can observe a narrow transmission peak that corresponds to the resonant mode of the cavity. The spectral position of the cavity mode is unambiguously confirmed by the far-field imaging, which allows one to identify the cavity resonance although the transmitted signal is weak or accompanied with spurious resonances. The cavity mode exhibits a stable, highly symmetric far-field pattern [see the inset in Fig. 2(b)] that

differs distinctly from the specklelike emission of the residual resonance peaks. A broad and weak resonance observed at 1580 nm between the cavity mode and the barrier cutoff was attributed to an evanescent mode, which can penetrate through the barriers due to evanescent coupling.

The light radiated from the sample surface and recorded as a function of the wavelength yields the emission spectrum of the cavity, which is shown in the inset of Fig. 2(b). It exhibits a better signal-to-noise ratio than the transmission and was, therefore, used to analyze the spectral properties of the cavity. The Lorentzian fit of the emission peak gives a linewidth of 60 ± 1 pm, yielding a loaded quality factor $Q = 26{,}000$.

To assess the sensing potential of the cavity, we expose the sample to gases of different refractive indices, such as air ($n = 1.000265$) [13], N_2 (1.000270) [14], He (1.000032) [13], and CO_2 (1.000407)[14]. The refractive index values are given at atmospheric pressure and were recalculated for $\lambda = 1570$ nm and room temperature $T = 20°$ C using the ideal gas model [15]. During the measurement, the sample is placed in a gas cell [see Fig. 2(a)] that is equipped with a gas inlet, 2 μm size openings for the optical fibers, and an outlet for gas evacuation. The gas is injected into the cell at a constant rate, fills the volume of the cell, and escapes by the outlet opening, thus avoiding the overpressure inside the cell. The flux rate is set to a value just sufficient to entirely fill the cell volume with the test gas by observing the shift of the cavity resonance upon accruing concentration of the gas; when a new increase of the gas flux does not induce further shift in the
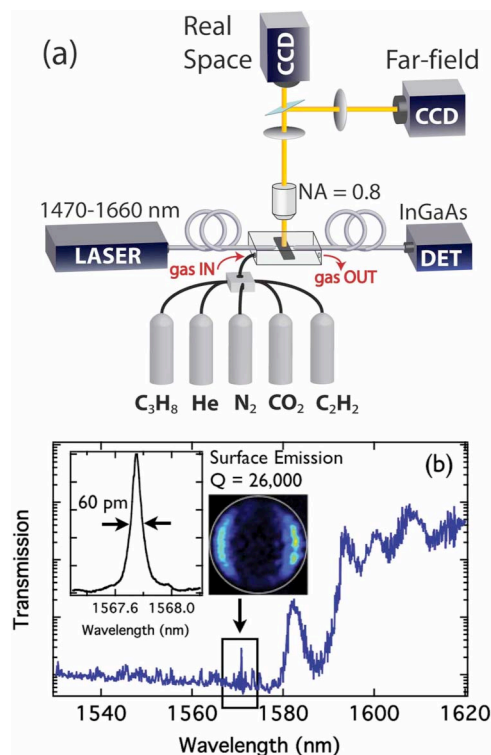

Fig. 2. (Color online) (a) Combined end-fire imaging setup. (b) Transmission spectrum of the air-slot cavity. Insets: surface emission spectrum (left) and the far-field image (right) at the cavity resonance.
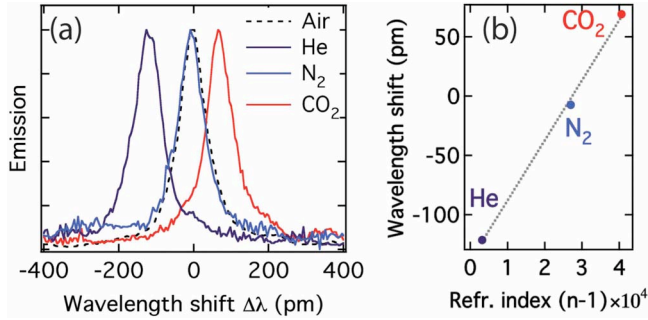
Fig. 3. (Color online) (a) Spectral position of the cavity resonance upon exposure to He, N_2, CO_2, and the air. (b) Wavelength shift of the cavity resonance as a function of the refractive index $(n-1)$ of the respective gas.

resonance wavelength, the cell is considered to be completely filled with the analyte.

The shift of the air-slot cavity resonance in response to the change of the gas refractive index is shown in Fig. 3. Considering air as the reference medium, we can observe both blue shift of the resonance peak for He and red shift for CO_2. As plotted in Fig. 3(b), the dependence of the wavelength shift on the refractive index change $(n-1)$ is strictly linear and yields the experimental sensitivity $\Delta\lambda/\Delta n = 510$ nm/RIU, which is slightly lower than predicted by the numerical analysis. The small discrepancy can be attributed to structural differences between the modeled and the fabricated device. Repetitive measurements on a longer time scale show that the peak position can be retrieved with a precision of ± 3 pm, which implies the detection limit (defined as the ratio between the resolution and the sensitivity) of 1×10^{-5} RIU. Nevertheless, it should be mentioned that along with the refractive index of the surrounding medium, there are other parameters that can induce a shift of the resonance frequency of the air-slot cavity mode, e.g., temperature, humidity adsorbed at the structure sidewalls, or progressive oxidation of the sample surface. In particular, the latter turns out to be the most detrimental, as it can induce a shift of the resonance peak by as much as 45 pm per hour. This effect can be eliminated when working with O_2-free gases, or compensated using an identical reference structure. Further enhancement of the sensor detection limit can be achieved by increasing the Q factor of the cavity, which improves the precision of the resonance frequency readout. However, note that the 40 aliters sensing volume holds as little as 1×10^6 molecules; With the present sensitivity and resolution limit, the sensor is less than an order of magnitude away from the mesoscopic regime,

where the effect of statistical fluctuations becomes significant and finally sets the physical limit of the sensor.

In conclusion, we have presented a highly sensitive refractive index detection scheme with a photonic crystal air-slot cavity. Because of a strong overlap of the cavity mode with the surrounding medium, such a cavity can achieve an experimental sensitivity of 510 nm/RIU with the detection limit higher than 1×10^{-5} RIU, which is comparable with state-of-the-art devices [3]. Yet, the major advantage of the sensor is an extremely small active sensing volume of 40 aliters, which is possible due to strong confinement of the optical field in PhC point-defect cavities. Such a small volume not only allows one to drastically decrease the necessary amount of analyte, but it also makes the sensor suitable for high-density integration oriented toward parallel or multiplex detection.

References

1. E. Kuramochi, M. Notomi, S. Mitsugi, A. Shinya, T. Tanabe, and T. Watanabe, Appl. Phys. Lett. **88**, 041112 (2006).
2. T. Asano, B. S. Song, Y. Akahane, and S. Noda, IEEE J. Sel. Top. Quantum Electron. **12**, 1123 (2006).
3. X. Fan, I. M. White, S. I. Shopova, H. Zhu, J. D. Suter, and Y. Sun, Anal. Chim. Acta **620**, 8 (2008).
4. M. Lončar, A. Scherer, and Y. Qiu, Appl. Phys. Lett. **82**, 4648 (2003).
5. W. Almeida, Q. X. Xu, C. A. Barrios, and M. Lipson, Opt. Lett. **29**, 1209 (2004).
6. J. T. Robinson, C. Manolatou, L. Chen, and M. Lipson, Phys. Rev. Lett. **95**, 143901 (2005).
7. A. Di Falco, L. O'Faolain, and T. F. Krauss, Appl. Phys. Lett. **94**, 063503 (2009).
8. T. Yamamoto, M. Notomi, H. Taniyama, E. Kuramochi, Y. Yoshikawa, Y. Torii, and T. Kuga, Opt. Express **16**, 13809 (2008).
9. J. Gao, J. F. McMillan, M. C. Wu, J. J. Zheng, S. Assefa, and C. W. Wong, Appl. Phys. Lett. **96**, 051123 (2010).
10. L. C. Andreani and D. Gerace, Phys. Rev. B **73**, 235114 (2006).
11. N. A. Mortensen, S. Xiao, and J. H. Pedersen, Microfluid. Nanofluid. **4**, 117 (2008).
12. N. Le Thomas, R. Houdré, M. V. Kotlyar, D. O'Brien, and T. F. Krauss, J. Opt. Soc. Am. B **24**, 2964 (2007).
13. L'Air Liquide, Division Scientifique, *Encyclopédie des Gaz* (Elsevier, 1976).
14. A. C. Simmons, Opt. Commun. **25**, 211 (1978).
15. Y. Clergent, C. Durou, and M. Laurens, J. Chem. Eng. Data **44**, 197 (1999).